Solid State Ionics 243 (2013) 8–17

Contents lists available at SciVerse ScienceDirect

Solid State Ionics

journal homepage: www.elsevier.com/locate/ssi

Structure, thermal stability and electrical conductivity of BINBVOX

E.S. Buyanova [a], M.V. Morozova [a,*], Ju.V. Emelyanova [a], S.A. Petrova [b], R.G. Zakharov [b], N.V. Tarakina [c,d], V.M. Zhukovskiy [a]

[a] Ural Federal University named after the first President of Russia B.N.Yeltsin, Department of Chemistry, Lenin Ave. 51, 620000, Ekaterinburg, Russia
[b] Institute for Metallurgy, Ural Branch of the Russian Academy of Sciences, Amundsen Str. 101, 620016, Ekaterinburg, Russia
[c] Institute of Solid State Chemistry, Ural Branch of the Russian Academy of Sciences, Pervomayskaya Str. 91, 620990, Ekaterinburg, Russia
[d] Experimentelle Physik III, Physikalisches Institut and Wilhelm Conrad Röntgen - Research Centre for Complex Material Systems, Universität Würzburg, Am Hubland, D-97074 Würzburg, Germany

ARTICLE INFO

Article history:
Received 10 April 2012
Received in revised form 3 April 2013
Accepted 9 April 2013
Available online 16 May 2013

Keywords:
BIMEVOX
Oxygen-ion conductors
Crystal structure
Polymorphic modifications
Electrical conductivity
Impedance spectroscopy

ABSTRACT

Materials based on BINBVOX compounds that are stable within wide concentration and temperature ranges have been synthesized. Refinement of the crystal structure of different BINBVOX modifications obtained at different temperatures and partial oxygen pressures has been carried out. The most promising solid solutions have been identified according to the linear dependence of the total electric conductivity on temperature and its independence on partial oxygen pressure.

1. Introduction

Solid solutions based on $Bi_4V_2O_{11}$ (or $Bi_2VO_{5.5}$) bismuth vanadate with vanadium partly substituted by another ME cation form the so-called BIMEVOX family, characterized by high oxygen-ion conductivity at intermediate temperatures. According to Ref. [1] the crystal structure of the parent bismuth vanadate can in general be described as alternating fluorite-like $(Bi_2O_2)^{2+}$ and perovskite-like $(VO_3\square_{0.5})^{2-}$ layers, where □ refers to structural vacancies in the anionic sublattice, which allow oxygen ions to migrate through the crystal. The $Bi_4V_2O_{11}$ compound crystallizes in four polymorphic modifications: α, β, γ and γ′. Phase transitions temperatures are about 450 °C (α↔β), 570 °C (β↔γ) and 870 °C (γ↔γ′). Most often, the highest electrical conductivity is observed for the high-temperature γ-modification of BIMEVOX, which can be stabilized at room temperature by substitution of V by dopants with different valence [1]. The tetragonal γ-$Bi_4V_2O_{11}$ modification contains 3 nonequivalent crystallographic oxygen positions: O(1) in the Bi_2O_2 layer, apical O(2), and O(3) in the basic plane of V–O polyhedrons. The O(2) and O(3) oxygen positions display the highest disorder in the structure [2]. Bismuth vanadates with V partly substituted by Nb have been the subject of only a few publications. The first work involving solid solutions of such a composition was made by O. Joubert et al. in 1994 [3] and revealed that $Bi_4V_{2-x}Nb_xO_{11}$ (BINBVOX) solid solution was limited to $x = 0.6$. In two more years Lazure et al. [4] found that $Bi_4V_{2-x}Nb_xO_{11}$ crystallizes in α, β, γ-modifications for $0 < x \le 0.15$, $0.15 < x \le 0.30$, and $0.30 < x \le 0.60$ dopant concentrations, respectively. Steil et al. [5] showed that the thermal stability of membranes made from BIMEVOX solid solutions with high valence dopants including $Bi_4V_{1.5}Nb_{0.5}O_{11}$ sample is much higher than that of the other solid solutions. The thermal expansion coefficient of $Bi_4V_{1.5}Nb_{0.5}O_{11}$ is equal to 14–14.5*10^{-6} K^{-1}. Impedance plots at low temperatures reveal larger resistance of grain boundaries than for other solid solutions, which is explained by the small size of the particles in the membrane. According to Ref. [6] low dopant concentrations, as for example in $Bi_4V_{1.9}Nb_{0.1}O_{11}$, leads to the formation of the orthorhombic α-modification, independently of the cooling rate during sample preparation. Long-term heating (200 hours at 600 °C) results in partial decomposition of the solid solution and the appearance of $BiVO_4$ and $Bi_{3.5}V_{1.2}O_{8.25}$ as impurities. The temperature dependence of the electrical conductivity of $Bi_4V_{1.9}Nb_{0.1}O_{11}$ displays inflections that correspond to γ↔β↔α reversible phase transitions.

Ref. [7] concerns the effect of partial substitution of V^{5+} sites by Nb^{5+} on the structural, optical and electrical properties of $B_4V_{2-x}O_{11}$ (BVO) thin films. The grain size, band gap width, refraction coefficient and dielectric constant of the films increase when the niobium concentration increases. This effect is attributed to the reduction of oxygen-ion vacancies [7].

* Corresponding author. Tel./fax: +7 343 2617411.
E-mail address: morphey_usu@mail.ru (M.V. Morozova).

0167-2738/$ – see front matter © 2013 Elsevier B.V. All rights reserved.
http://dx.doi.org/10.1016/j.ssi.2013.04.009

The present work involves the synthesis, the crystal structure, the thermal stability and the electrical conductivity of the $Bi_4V_{2-x}Nb_xO_{11}$ solid solution within a wide range of thermodynamical parameters.

2. Experimental

The synthesis of $Bi_4V_{2-x}Nb_xO_{11}$ was performed by both the standard ceramic technology and the co-precipitation method. The ceramic synthesis was carried out using Bi_2O_3 (99.9%), V_2O_5 (99.9%) and Nb_2O_5 (99.9%) initial oxides in the temperature range 500–800 °C with 50 °C step and 8–10 hours of sintering at each stage. The synthesis through the co-precipitation method involved the preparation of bismuth nitrate $Bi(NO_3)_3$ and ammonium metavanadate NH_4VO_3 solutions by dissolving solid salts in distilled water to which concentrated nitric acid was added. Niobium, in the form of pentabutoxi-niobium $C_{20}H_{45}O_5Nb$, was added to the continuously stirred reaction solution. The NH_4OH precipitator was added to get a pH of 9–10. The obtained precipitate was settled during 30 minutes and then dried at 200 °C. Final annealing was carried out at 700 °C during 4–5 hours, then the samples were slowly cooled with the furnace (about 5 deg/h). The phase composition of the final solid oxide products was checked by X-ray powder diffraction (DRON-3 diffractometer, CuK_α-radiation, pyrolytic carbon monochromator, reflected beam). For a precise and detailed high-temperature crystal structure study the powder diffraction patterns were collected on a D8 ADVANCE diffractometer equipped with VÅNTEC1 PSD and Anton Paar HTK1200N high-temperature chamber, using filtered CuK_α radiation. Phase analysis, indexing of the collected diffraction patterns and refinement of the crystal structure were performed using the LMGP [8] and TOPAS [9] software packages. Taking into account the intricate phase composition of the majority of samples phase analysis was based on the whole-pattern analysis with the appropriate structural models [10] involved in the refinement. Frequency characteristics of metal–oxygen bonding were measured by means of IR Fourier spectroscopy (Nicolet 6700 spectrometer, diffusion reflection method). Particle sizes were determined using a SALD-7101 Shimadzu particle-size analyzer. Thermal dilatometric analysis was performed in the temperature range 20 – 650 °C with a heating rate of 2 deg/min on a DIL 402 C Netzsch dilatometer equipped with a vacuum furnace. The samples for dilatometric analysis were previously sintered at 800 – 830 °C. Differential thermal analysis was carried out using a STA 409 PC Luxx Netzsch thermal analyzer within the 20 – 700 °C temperature range. Aluminium oxide was used as a reference material. For subsequent analysis, the obtained powders were pressed into pellets and annealed at 820 °C during 2 hours. The morphology of the obtained powders and their chemical composition have been studied using a JEOL JSM6390 LA scanning electron microscope equipped with a JED-2300 energy dispersive X-ray detector.

For the electrical conductivity study, the annealed pellets were polished and coated with ammonium hexacloroplatinate $(NH_4)_2PtCl_6$ to obtain platinum electrical contacts. Electrical conductivity measurements of ceramic samples were performed on Elins Z-2000 and Elins Z-350M impedance spectrometers in the temperature range 200 – 800 °C and oxygen partial pressure in the range 0.21 – 10^{-6} (atm).

3. Results

3.1. Crystal structure and thermal characteristics of BINBVOX

Both the ceramic and the co-precipitation synthesis result in the formation of $Bi_4V_{2-x}Nb_xO_{11}$ solid solutions with x up to 0.9, which is a wider range than reported in Refs. [3–5]. Nevertheless our data correspond to BINBVOX solid solution limits calculated by I. Abrahams and F. Krok [11] according to two different defect structure models: Bi_4VMeO_{11} assuming the equatorial vacancy limiting model or $Bi_4V_{0.5}Me_{1.5}O_{11}$ assuming the apical one. These calculations were made for 5+ charged dopant metal ion at vanadium site and its coordination number CN = 6. Therefore solid solution range x up to 0.9 reported in the present paper lies within the theoretically predicted limits. For the co-precipitation method (maximum annealing temperature 700 °C), low niobium concentrations ($x < 0.20$) lead to the formation of the monoclinic α-modification of the solid solution (space group $C2/m$). Dopant concentrations $0.2 \le x \le 0.3$ under the same synthesis conditions lead to the additional formation of the orthorhombic β-modification with doubled a parameter of the unit cell ($a = 2a_m$), thereby reflections of both modifications are seen in the X-ray patterns (Fig. 1). Insets in Fig. 1 clarify the presence of both the monoclinic distortion and orthorhombic modification. The splitting of the $(220)_m$ and $(206)_m$ peaks for monoclinic phase together with the $(122)_o$ and $(006)_o$ peaks of the orthorhombic modification are shown. For dopant

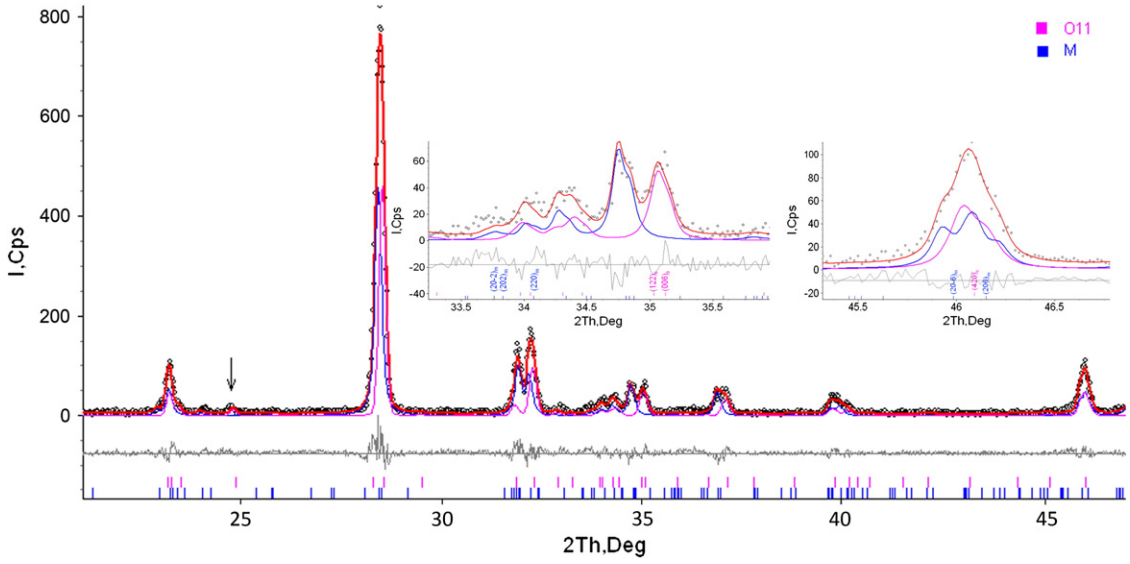

Fig. 1. A fragment of the diffractogram of the $Bi_4V_{2.8}Nb_{0.2}O_{11}$ solid solution produced by the co-precipitation method and consisted of two phases: monoclinic (M) and orthorhombic one (O11). An arrow indicates the reflection of the orthorhombic cell which can be indexed through doubling a parameter only. The insets show splitting of the $(220)_m$ and $(206)_m$ peaks for monoclinic phase together with the $(122)_o$ and $(006)_o$ peaks of the orthorhombic modification.

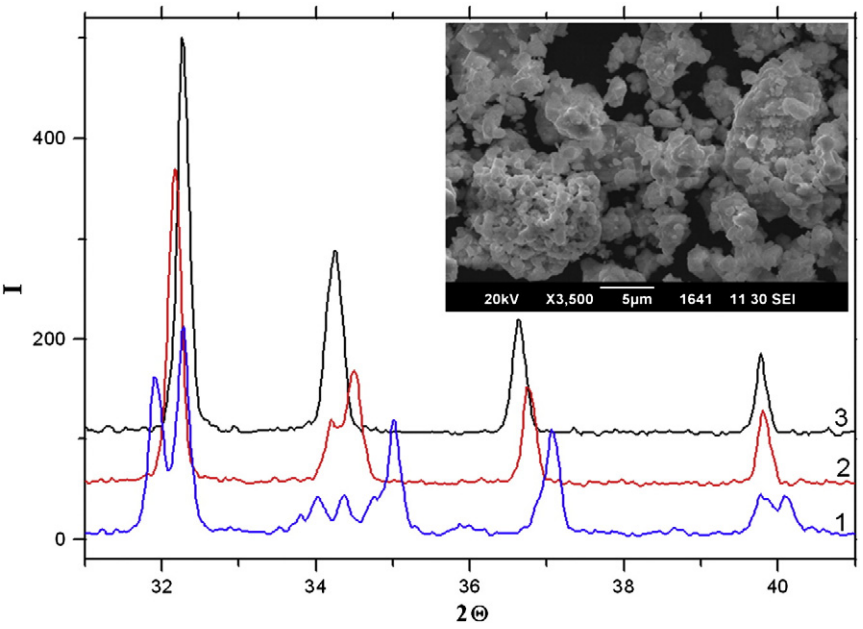

Fig. 2. Characteristic regions of the X-ray patterns of $Bi_4V_{2-x}Nb_xO_{11}$ obtained by co-precipitation method: 1 – $x = 0.1$; 2 – $x = 0.2$, 3 – $x = 0.6$ and the SEM image of the $x = 0.6$ sample.

concentrations larger than 0.5 only the tetragonal γ-structure is formed. The ceramic synthesis with maximum annealing temperature 800 °C allows to obtain a mixture of monoclinic and orthorhombic modifications without any doubling of unit cell parameters up to $x = 0.30$. At $0.3 < x < 0.4$, the formation of a mixture of orthorhombic and tetragonal modifications is observed. The high-temperature γ-modification of the $Bi_4V_{2-x}Nb_xO_{11}$ solid solution (space group $I4/mmm$) is obtained at $0.4 \leq x \leq 0.9$ niobium concentration range. The X-ray patterns of the samples are alike for different compositions but the same polymorph modifications. Fig. 2 shows examples of polymorphic modifications diffractograms and a SEM image of $x = 0.6$ powder synthesized through the co-precipitation method. The particle sizes vary obviously but no extra phases are seen in the SEM image. X-ray patterns of the $x = 0.9$ sample prepared using different synthesis methods are given in Fig. 3 and reveal the similarity of the structure while unit cell parameters differ significantly. For solid solution synthesized via ceramic

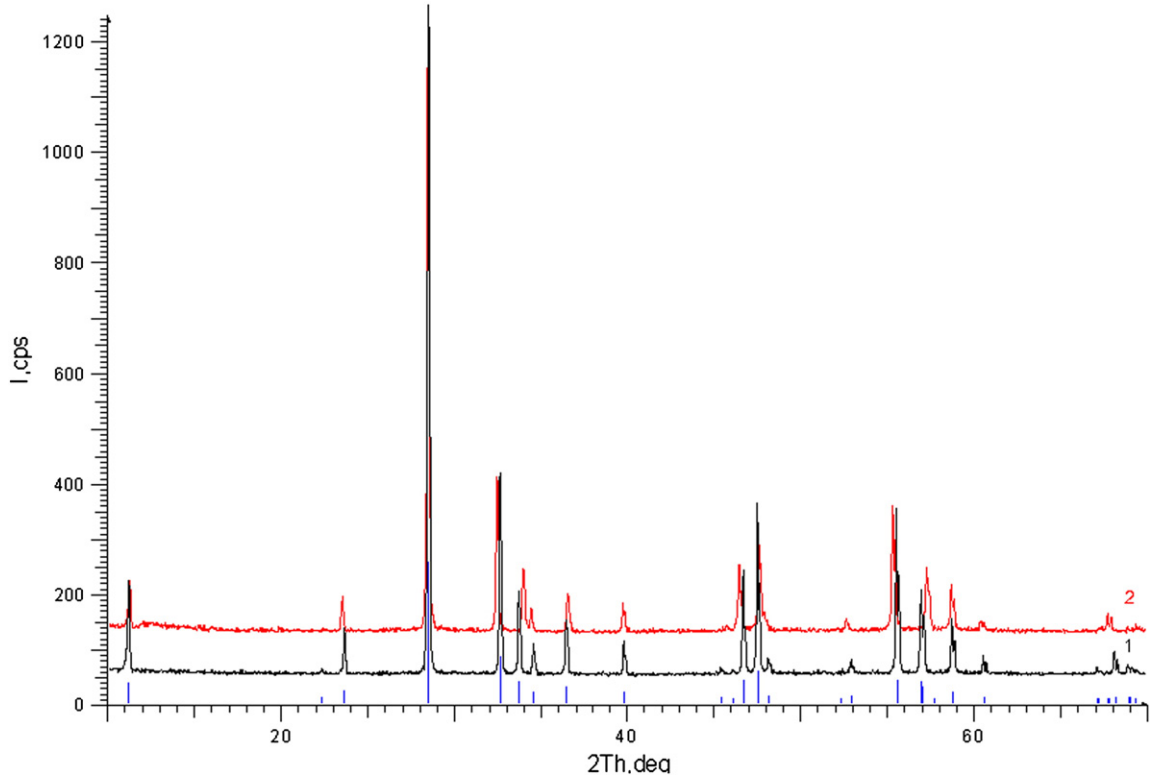

Fig. 3. The diffractograms of two $Bi_4V_{2.1}Nb_{0.9}O_{11}$ solid solutions synthesized by both the standard ceramic technology (1) and the co-precipitation method (2) together with Bragg positions for a tetragonal modification.

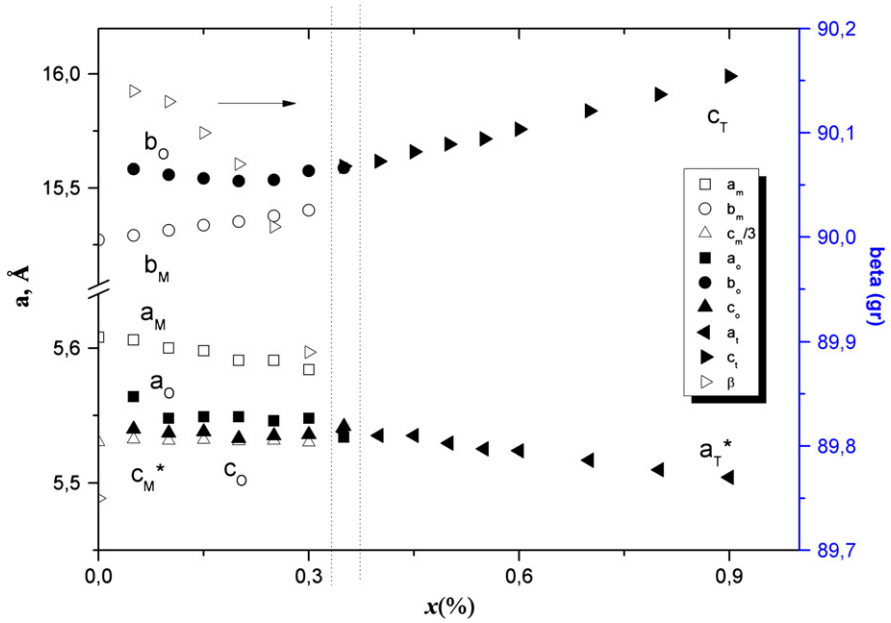

Fig. 4. Crystallographic characteristics of the $Bi_4V_{2-x}Nb_xO_{11}$ solid solution synthesized via standard ceramic technology. By indexes "m", "o", and "t" unit cell parameters of monoclinic, orthorhombic and tetragonal phases are indicated. For better view modifying parameters $c_m^* = c_m/3$ and $c_t = \sqrt{2}c_t$ are used.

route, (Fig. 3, curve 1), $a = 3.8925(2)$Å, $c = 15.9908(10)$Å, $V = 242.291(24)$Å^3 and for the co-precipitation method (Fig. 3, curve 2), $a = 3.9089(2)$Å, $c = 15.8678(11)$Å, $V = 242.457(28)$Å^3. According to the Rietveld full-profile refinement we can assume that it results from various configuration of O–(Nb,V)–O groups in (V, Nb –O) layers (angles and bonds length) but a precise conclusion requires additional neutron investigations. Fig. 4 shows the dependence of the unit cell parameters of the $Bi_4V_{2-x}Nb_xO_{11}$ solid solution synthesized by the standard ceramic technology on dopant content; different crystal structure modification ranges are marked.

The frequency characteristics of the metal–oxygen bonds were determined by means of IR Fourier spectroscopy. The primary characteristic bands are listed in Table 1.

IR spectra of the parent compound, α-$Bi_4V_2O_{11}$, and the BINBVOX solid solutions are characterized by a set of absorption bands referred to the valence and deformation vibrations of V–O bonds in VO_4 tetrahedra, O–V–O groups in $(VO_{3.5}\square_{0.5})^{2-}$ layers and to the Bi–O vibrations in Bi_2O_2 layers (Table 1). The data correlate to the results obtained by Alga et al. [12] and prove mainly tetrahedral coordination of vanadium atoms. The presence of asymmetrical vibrations indicates possible deformation of V–O polyhedrons. An increase of dopant concentration is accompanied by a decrease of both intensity of V–O asymmetrical valence vibrations and frequency of symmetric vibrations. As it was found for other BIMEVOX solid solutions (ME – Ca, Hf) [13,14] such a change of IR spectra may argue the incorporation of dopant atoms (in our case Nb) into vanadium sites within VO_4 polyhedrons.

Solid solutions with high concentrations of Nb ($x = 0.9$) are characterized by the presence of an extra band at 845 cm^{-1} which corresponds to vibrations of the Nb–O group [15]. The absence of asymmetrical valence vibrations for $x \geq 0.4$ results from initial structural distortion as was shown in Ref. [16]. It correlates well with the results of our crystal structure study according to which the most disordered tetragonal γ-modification of BINBVOX is formed at $x \geq 0.4$.

The size of the obtained powders depends on the synthesis route. The use of the co-precipitation method results in powders with an average grain size of 0.5–5 μm which is one order of magnitude lower than that obtained for the ceramic synthesis.

An investigation of BINBVOX polymorphism was carried out by means of dilatometric, thermal and high-temperature X-ray methods. The BINBVOX samples that crystallize in the α- or the β-modification at room temperature are characterized by a rather wide hysteresis of heating and cooling linear thermal expansion curves. Fig. 5 shows an example of such curves for the $Bi_4V_{1.9}Nb_{0.1}O_{11}$ solid solution. The sharp step at 200–300 °C corresponds to the α↔β phase transition. The slight dip at 500 °C is characteristic for a phase transition into the γ-modification. The linear thermal expansion curves of γ-BINBVOX for heating and cooling almost coincide. The absence of the above mentioned phase transitions is clearly seen for samples with tetragonal γ-structure (for example, $x = 0.9$, see Fig. 6), though a very slight change of slope is observed at 400 – 500 °C and it is usually identified as a γ↔γ' (order – disorder type) transition. As it can be seen the value of the linear thermal expansion coefficient of BINBVOX samples is equal to (15–21)*10^{-6} K^{-1} (at 550–700 °C) and lowers with increase of dopant concentration (Fig. 7).

The absence of α↔β, β↔γ phase transitions and the emission of gaseous products during heating and cooling of the γ-modification samples was demonstrated by means of the TG/DSC method (Fig. 8). A small endothermic peak is also observed at 570 °C which corresponds to the γ↔γ' transition.

A high-temperature X-ray powder diffraction study of the BINBVOX samples did not reveal sharp phase transitions for compositions with $x = 0.6$ and 0.9 synthesized via the ceramic method within the temperature range 25–830 °C in air. As an example, Fig. 9 shows X-ray patterns of $Bi_4V_{1.4}Nb_{0.6}O_{11}$ at different temperatures of the heating–cooling cycle with the same slight change of the main Bragg peaks that could be due to γ↔γ' transition.

To determine the decomposition temperature of BINBVOX compounds and the region of their stability within a wide range of partial oxygen pressures (Po_2), high-temperature X-ray investigations at different Po_2 pressures for $Bi_4V_{1.4}Nb_{0.6}O_{11}$ and $Bi_4V_{1.1}Nb_{0.9}O_{11}$ synthesized

Table 1
Characteristic bands of $Bi_4V_{2-x}Nb_xO_{11}$ IR spectra.

x	ν_s (V–O), cm^{-1}	ν_{as} (V–O), cm^{-1}	δ_{as} (O–V–O), cm^{-1}	ν (Bi–O), cm^{-1}	ν (Nb–O), cm^{-1}
0.0	742	930, 854	571, 484	435, 427, 417	
0.1	715	927	609, 472	448, 401	
0.4	705, 702	-	656	416, 403	
0.9	684		615, 496	403	845

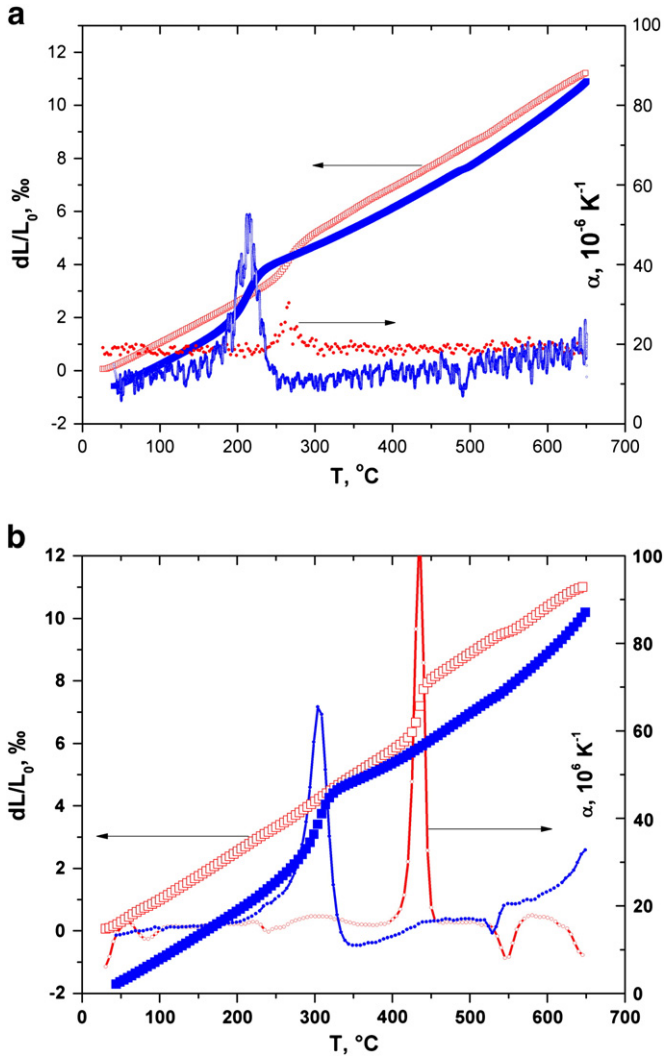

Fig. 5. Dilatometric analysis data for $Bi_4V_{1.9}Nb_{0.1}O_{11}$: a) co-precipitation synthesis method; b) standard ceramic technology. Open signs – heating; solid signs – cooling. Heating–cooling rate – 2 deg/min.

via the standard ceramic technology were performed. Fig. 10 shows temperature dependences of the unit cell parameters of the samples at different Po_2 values. Heating was carried out at $lgPo_2 = -0.67$ (atm),

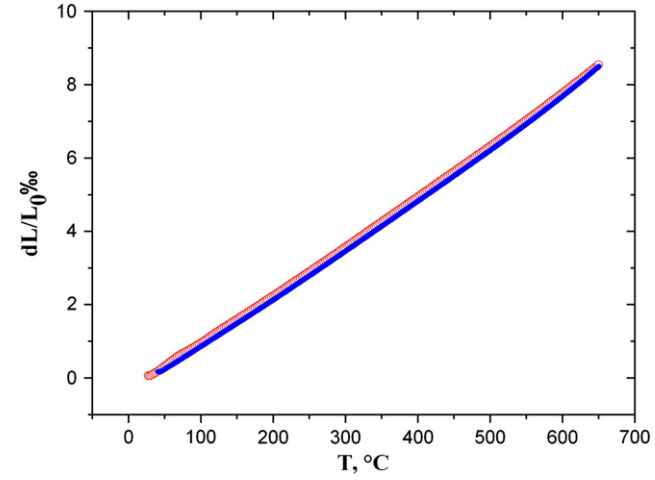

Fig. 6. Dilatometric analysis data for $Bi_4V_{1.5}Nb_{0.9}O_{11}$ (co-precipitation method of synthesis). Open signs – heating; solid signs – cooling.

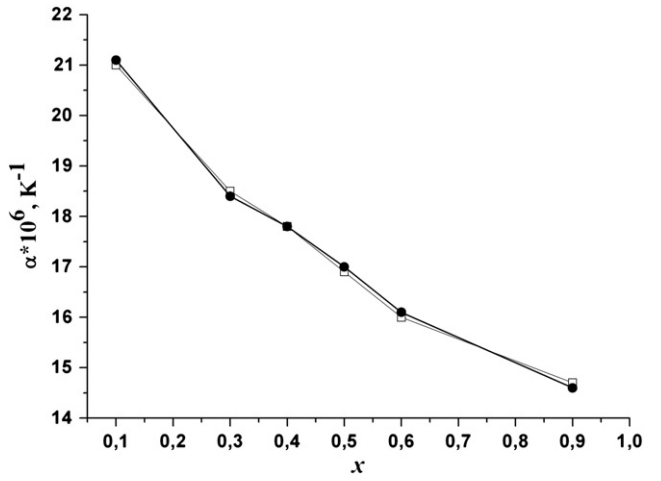

Fig. 7. Linear thermal coefficients values of BINBVOX solid solutions synthesized by different methods. Open signs – co-precipitation synthesis; solid signs – ceramic synthesis.

cooling at $lgPo_2 = -2$ (atm). Such experimental conditions were chosen for a further possibility to compare the behavior of the samples under precise partial oxygen pressure with "ambient air" ($Po_2 = -0.67$) and/or "light" vacuum ($Po_2 = -2$) together with the temperature change. The discrepancy in the unit cell parameters for heating and cooling at different oxygen partial pressures is attributed to the interaction of the samples with residual oxygen of the environment due to the vacancies in the oxygen sublattice. The behavior of unit cell parameters of the studied compounds is linear at different partial oxygen pressures. An increase of dopant concentration up to the highest value of the homogeneity range ($x = 0.9$) makes the situation more complicated since the spread of the experimental points in the graph of the temperature dependence of unit cell parameters exceeds the error in the unit cell parameters determination. Most likely this can be explained by a distortion of the tetragonal cell with temperature, which results in a broadening of certain reflections on the X-ray powder patterns (Fig. 11). Indeed, annealing of the samples with $x = 0.5$–0.9 at 830 °C leads to much higher values of the full width at half maximum for the (006), (015) and (118/019) reflections compared to others.

A plot of the unit cell parameters of the $x = 0.6$ solid solution versus partial oxygen pressure within the 750–780 °C temperature range is shown in Fig. 12. The linearity of the $a(b,c) = f(\lg Po_2)$ curve breaks down at pressures lower than $lgPo_2 = -12$ (atm). X-ray powder diffraction patterns reveal the presence of Bi_2O_3 impurity at

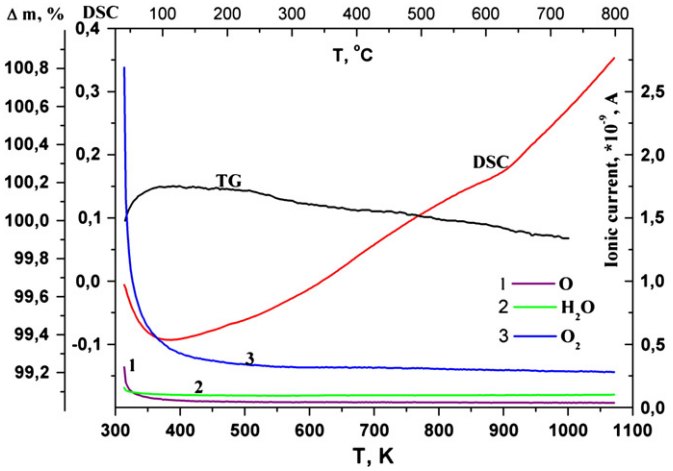

Fig. 8. TG and DSC curves (left scales) and mass spectrometric detection of fractions (right scale) with mass equal to 16 (O); 18 (H_2O); 32 (O_2) while heating the sample for $Bi_4V_{1.4}Nb_{0.6}O_{11}$ (ceramic synthesis).

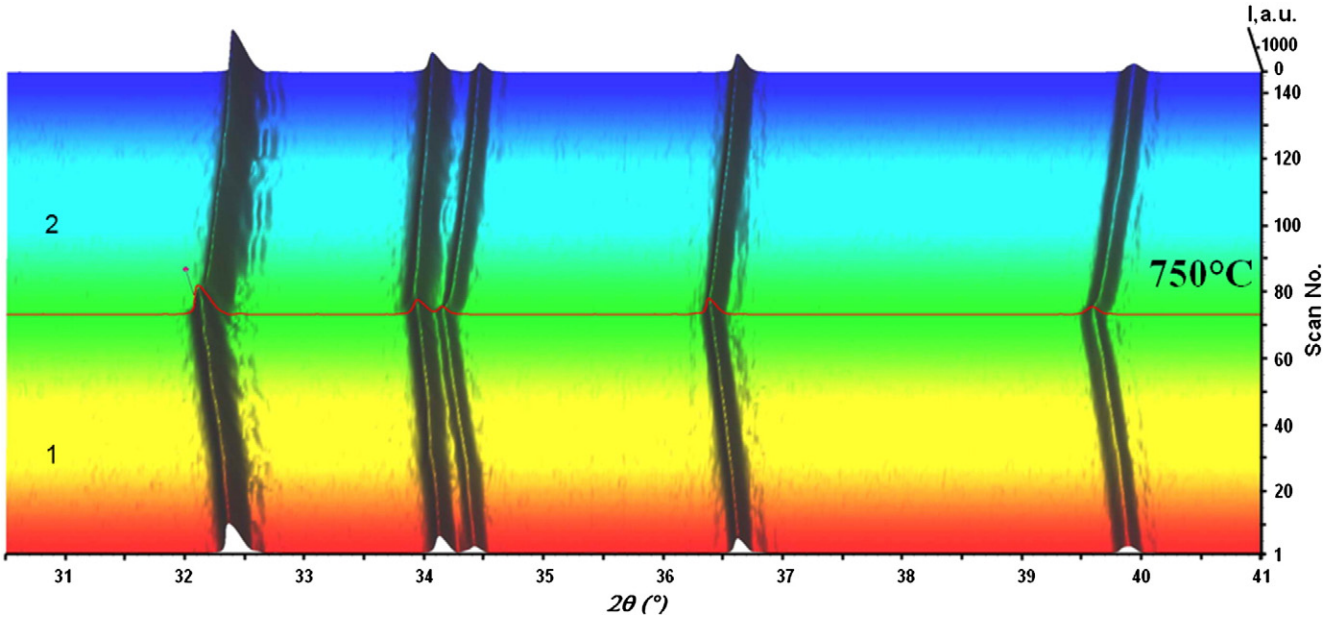

Fig. 9. High-temperature X-ray patterns of $Bi_4V_{1.4}Nb_{0.6}O_{11}$ within 30–750 °C range (heating–cooling, temperature change rate – 0.5 deg/sec.): 1 – heating region; 2 – cooling redion.

$lgPo_2 = -17$ (atm). The linear dependence of the unit cell parameters is primarily due to the escape of oxygen atoms from the crystal lattice, and the change of the slope is due to a change of metal atoms ratio while retaining the parent structure symmetry.

The above conclusion has been made on the basis of our previous investigations of other oxides under low partial oxygen pressure. For example, for manganese oxides it was established that the temperature of formation of monoxide decreases by several hundred degrees

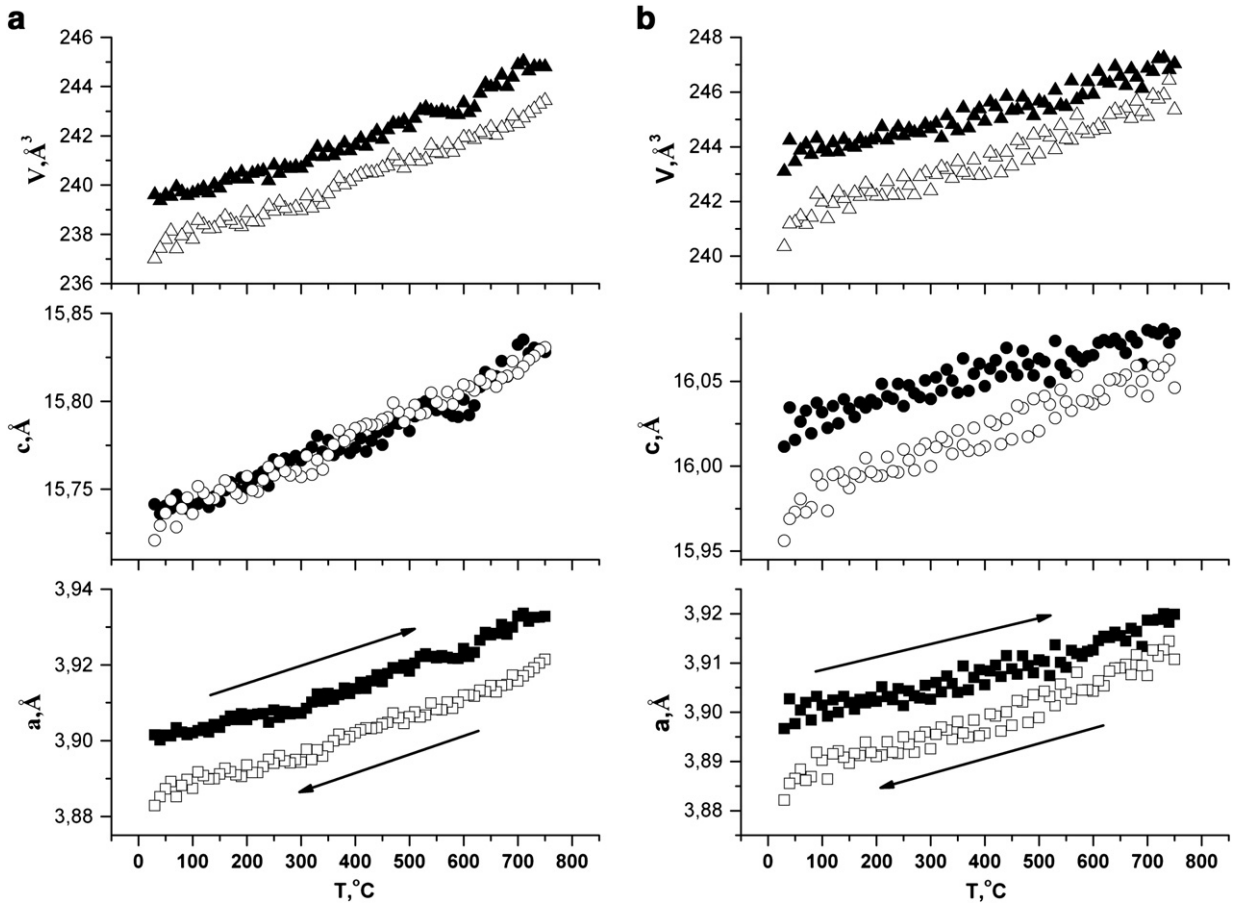

Fig. 10. Unit cell parameters values of $Bi_4V_{2-x}Nb_xO_{11}$: *а*) $x = 0.6$; *б*) $x = 0.9$. Open points – cooling at $lgPo_2 = -2$ (atm); solid points – heating at lg $Po_2 = -0.67$ (atm).

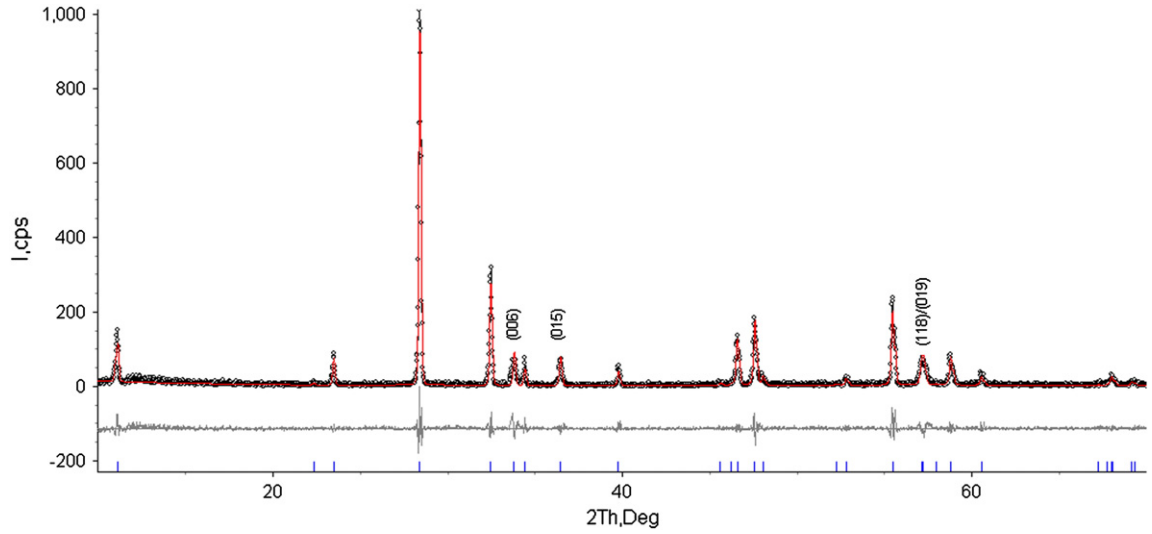

Fig. 11. The diffractogram of the $Bi_4V_{2.2}Nb_{0.8}O_{11}$ solid solution synthesized by standard ceramic technology at 830 °C that is characterized by selective broadening of some reflections.

with decreasing partial oxygen pressure below $lg(Po_2) = -10$. More details about experimental equipment are described elsewhere [17]. Equilibrium time at single oxygen partial pressure varied around one–two hours depending on the time required to stabilize values of current and voltage of the "pump-sensor" system.

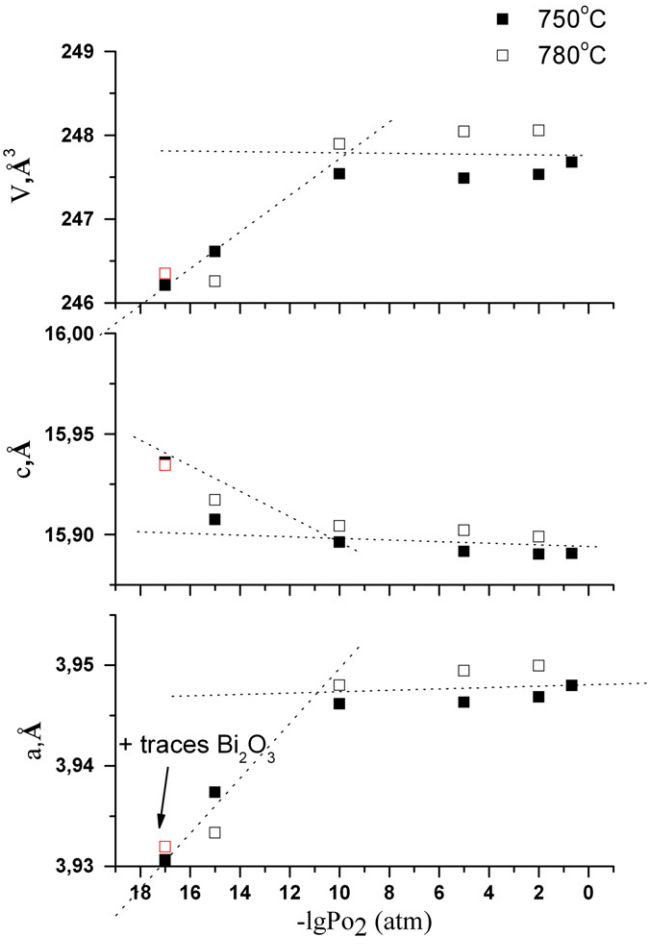

Fig. 12. $Bi_4V_{1.4}Nb_{0.6}O_{11}$ solid solution unit cell parameters plot versus partial oxygen pressure.

To investigate the total conductivity, pellets were formed from the BINBVOX powders and their density was checked to be not less than 90%. As an example, Fig. 13 shows the surface of a $Bi_4V_{1.1}Nb_{0.9}O_{11}$ pellet formed from powders synthesized via the co-precipitation method.

3.2. Electrical conductivity of BINBVOX

Complex plane plots of the BINBVOX solid solutions consist of two joint half-circles showing behavior typical for ionic conductors. Fig. 14(a, b) shows examples of complex plane plots of $Bi_4V_{1.6}Nb_{0.4}O_{11}$ at different temperatures. Modeling of the plots was performed using the equivalent electrical circuits method.

The equivalent electrical circuit consists of the following elements at temperatures >350 °C: R1, corresponding to the total resistance of the bulk and grain boundaries, connected in parallel to a complex of R2/CPE2 (constant phase element) and W2 (Warburg element). The CPE element is a constant phase element. It consists of two parts—CPE-T (Ohm) and CPE-P—which is equal to the order of magnitude. It describes complex processes and can stand for resistance or capacitance depending on the value of the CPE-P element. Warburg element in the equivalent circuits stands for complex processes that take place in the

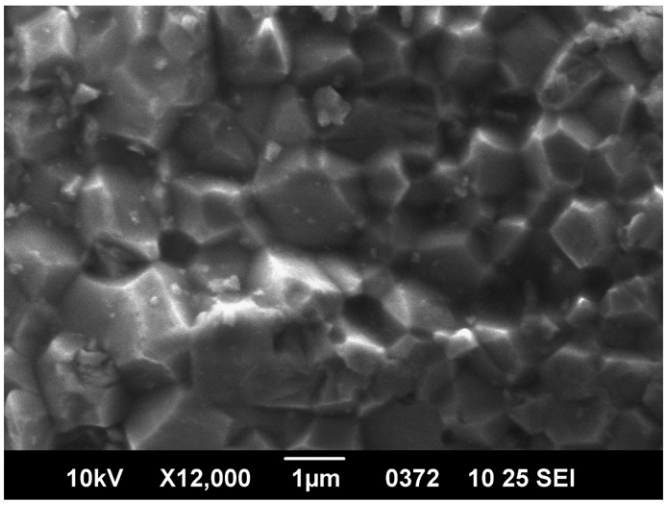

Fig. 13. Photomicrography of the $Bi_4V_{1.1}Nb_{0.9}O_{11}$ briquette surface.

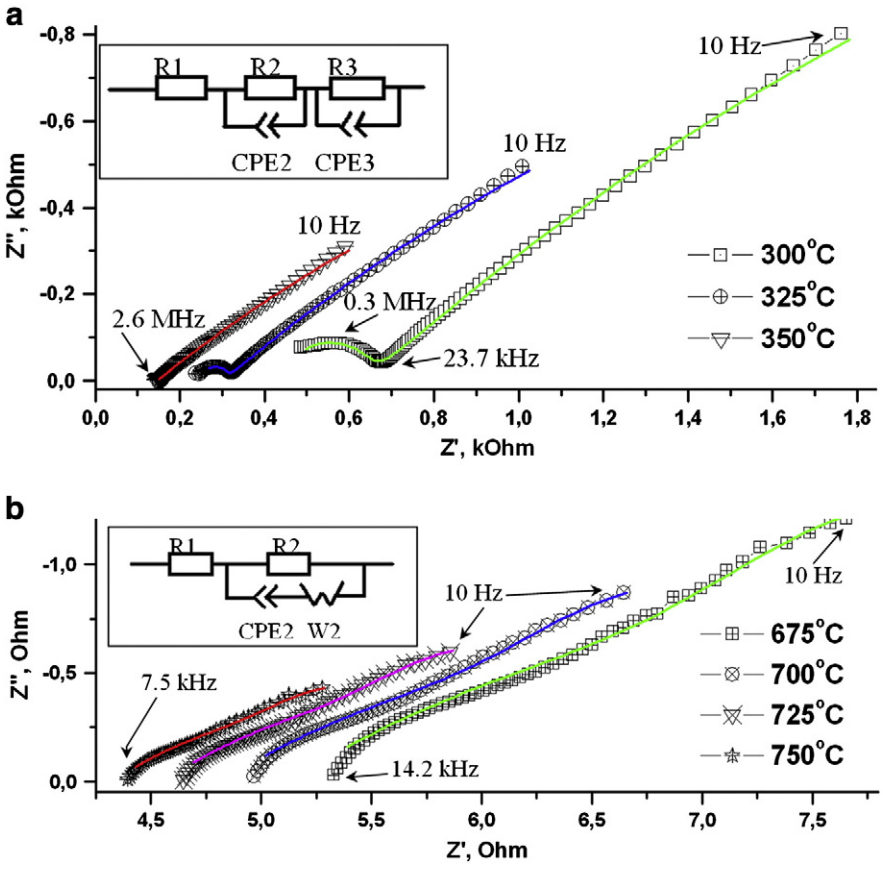

Fig. 14. Equivalent electrical circuits and results of the complex plane plots modeling of the Pt/BINBVOX/Pt electrochemical cell: a – low temperatures; b – high temperatures.

electrode–electrolyte border and inside the electrodes and can describe diffusion, or electrochemical reactions, polarization and other. It consists of three components, which can be assigned to overall resistance (Ws-R) and complex capacitance (Ws-T, Ws-P) of these processes. For temperatures lower than 350 °C the circuit is represented by a series connection of one resistance and two Voight elements (R/CPE). In this case the R1 and R2/CPE2 elements correspond to the bulk resistance of the crystallites and to the grain boundary resistance, respectively. Numerical parameters of the circuits are listed in Table 2. Fitting results were used first of all to define the value of total resistance of samples. The temperature dependence of the electrical conductivity of the BINBVOX solid solution polycrystalline samples was calculated from the impedance spectroscopy data. The total resistance was determined from the complex plane plots as a sum of bulk and grain boundary components.

Table 2
Equivalent circuits parameters that describe typical BINBVOX solid solutions complex plane plots.

Element of the equivalent circuit	Temperature		
	675 °C	650 °C	350 °C
R1, Ohm	10.9	12.3	85
R2, Ohm	83.6	243.1	3486
CPE2-T, F	$6.1*10^{-3}$	$4.1*10^{-3}$	$1.34*10^{-10}$
CPE2-P	0.45	0.44	0.90
R3, Ohm	-	-	$3.65*10^{4}$
CPE3-T, F	-	-	$1.1*10^{-5}$
CPE3-P	-	-	0.39
$W2_s$-R, Ohm	12.6	7.46	-
$W2_s$-T, F	$8.8*10^{-4}$	$5.4*10^{-4}$	-
$W2_s$-P	0.31	0.31	-

Typical temperature dependences of the total conductivity of the BINBVOX solid solution synthesized by various methods are shown in Fig. 15. Small dopant concentrations result in a sharp decrease of the total conductivity in the temperature range 480–420 °C which accompanies the phase transition. These data correlate well with the results of structural, thermal and dilatometry investigations. The temperature dependences of the total conductivity of the samples with γ-structure are characterized by a small change in slope when a transition into the γ-modification takes place while cooling.

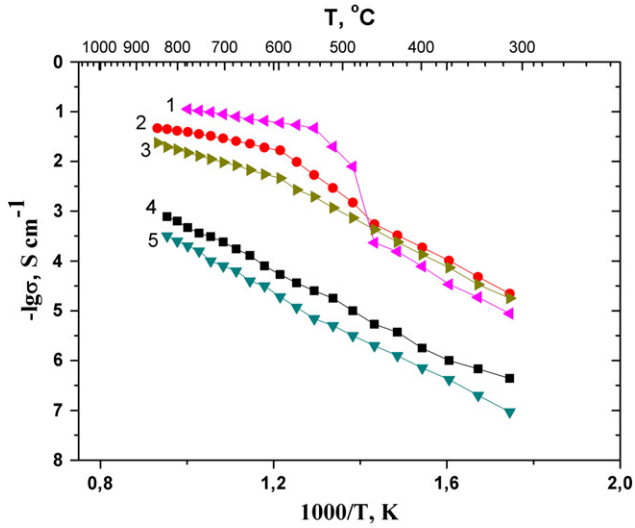

Fig. 15. Arrhenius plot of total conductivity for BINBVOX. 1 – ceramic synthesis, $x = 0.1$; 2 – ceramic synthesis, $x = 0.2$; 3 – ceramic synthesis, $x = 0.6$; 4 – co-precipitation synthesis, $x = 0.8$; 5 – ceramic synthesis, $x = 0.8$.

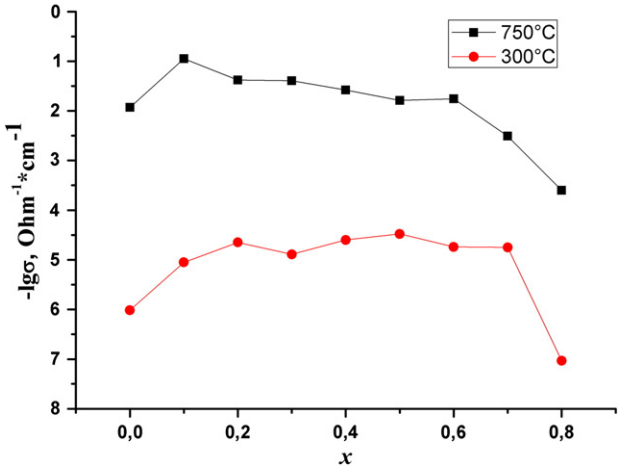

Fig. 16. Total electrical conductivity plots of BINBVOX at different Nb concentration and temperature values.

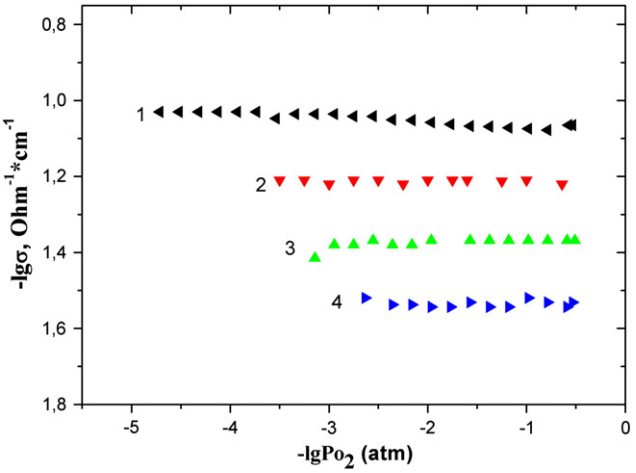

Fig. 17. Total conductivity plots of $Bi_4V_{1.6}Nb_{0.4}O_{11}$ upon partial oxygen pressure at different temperatures: 1 – 800 °C; 2 – 700 °C; 3 – 650 °C; 4 – 600 °C.

The total electrical conductivity of the samples synthesized by the co-precipitation method is higher than that of the solid-state samples. It is reflected in the complex plane plots as a shift of curves towards the high frequency range and a decrease of the diameter of the semi-circle representing grain boundary conductivity. Fig. (16) shows total conductivity of the samples with different dopant concentrations x synthesized using the ceramic method and the Table 3 contains values of the activation energy of the samples. The highest conductivity at medium temperatures is a characteristic of low dopant concentrations ($x < 0.3$) and it shows a typical tendency of the BIMEVOX family. As it was shown in Ref. [18], the increase of the total conductivity at isovalent substitution of vanadium by niobium can be due to local strengthening of the Nb–O bonds in the first coordination sphere of niobium atoms compared to the V–O bonds and to a slight decrease of the V–O(2) interaction in comparison with the undoped γ-$Bi_4V_2O_{11}$. Therefore, the insertion of niobium into the γ-$Bi_4V_2O_{11}$ structure should result in an increase of the participation of O(2) oxygen atoms in ionic conductivity.

The dependence of the total conductivity on the partial oxygen pressure at different temperatures for $Bi_4V_{1.6}Nb_{0.4}O_{11}$ sample is shown in Fig. 17. At low values of oxygen activity complex plane plots display a similar change in behavior as it was observed at low temperatures. The plots can be described using the same typical equivalent circuits mentioned above.

The electrical conductivity dependences on the partial oxygen pressure are linear within the investigated Po_2 range. This fact indicates that the electrical conductivity of the considered solid solutions is primarily oxygen-ionic and correlates with the data obtained in Ref. [6].

Table 3
Electrophysical characteristics of BINBVOX.

x	$E_{act.} \pm 0.02$, eV	$E_{act.} \pm 0.02$, eV
	>600 °C	<400 °C
0.1	0.25	0.94
0.2	0.25	0.89
0.3	0.28	0.81
0.4	0.33	0.86
0.5	0.47	0.87
0.6	0.49	0.88
0.7	0.61	0.75
0.8	0.81	0.84

4. Conclusions

The present work deals with the synthesis of the $Bi_4V_{2-x}Nb_xO_{11}$ solid solutions using ceramic and co-precipitation methods. The use of liquid precursors allows one to decrease the temperature and the duration of the synthesis process and to get powders with smaller grain size. The border of the $Bi_4V_{2-x}Nb_xO_{11}$ homogeneity range was determined to be equal to $x = 0.9$. The concentration ranges of different structural modifications were also determined. The high-temperature γ-$Bi_4V_{2-x}Nb_xO_{11}$ modification (space group $I4/mmm$) is formed at $0.3 \le x \le 0.9$ niobium content irrespective of the synthesis method. High-temperature X-ray powder diffraction analysis and dilatometry revealed some specific features of polymorphism in $Bi_4V_{2-x}Nb_xO_{11}$. The lowest partial oxygen pressure value within the stability range of BINBVOX at 750 °C was determined to be about $lgPo_2 = -12$ (atm). Further lowering of the partial oxygen pressure results in the decomposition of the solid solutions accompanied by the formation of bismuth oxide. The total conductivity of BINBVOX was investigated using electrochemical spectroscopy. The modeling of impedance spectra was performed within the same temperature ranges as for the total conductivity measurements. They were found to be linear for the γ-modification samples. The highest conductivity values are characteristic for small dopant concentration solid solutions ($x < 0.3$). The dependence of the total conductivity on the partial oxygen pressure within $10^{-6} \le Po_2 \le 0.21$ (atm) at T > 600 °C was found to be linear, indicating that the electrical conductivity of $Bi_4V_{2-x}Nb_xO_{11}$ solid solutions within the considered ranges is primarily oxygen-ionic.

Acknowledgments

This work was financially supported by the Russian Federal Agency for Education and Science within the "Scientific, research and educational personnel of innovative Russia, 2009–2013" federal program and the Ural Federal University development program for the financial support of young scientists. N.V.T. acknowledges funding by the Bavarian Ministry of Sciences, Research and the Arts.

References

[1] F. Abraham, J. Boivin, G. Mairesse, G. Nowogrocki, Solid State Ionics 40–41 (1990) 934.
[2] G. Mairesse, P. Roussel, R.V. Vannier, M. Anne, C. Pirovano, G. Nowogrocki, Solid State Sci. 5 (2003) 851.
[3] O. Joubert, A. Jouanneaux, M. Ganne, R.N. Vannier, G. Mairesse, Solid State Ionics 73 (1994) 309.

[4] S. Lazure, Ch. Vernochet, R.N. Vannier, G. Nowogrocki, G. Mairesse, Solid State Ionics 90 (1996) 117.
[5] M.C. Steil, F. Ratajczak, E. Capoen, C. Pirovano, R.N. Vannier, G. Mairesse, Solid State Ionics 176 (2005) 2305.
[6] Y. Taninouchi, T. Uda, T. Ichitsubo, Y. Awakura, E. Matsubara, Solid State Ionics 181 (2010) 1279.
[7] N. Kumari, K.B.R. Varma, S.B. Krupanidhi, Mater. Sci. Eng. B 153 (2008) 36.
[8] J. Laugier, B. Bochu, LMGP-Suite of Programs for the interpretation of X-ray Experiments. ENSP, Lab. Materiaux Genie Phys, Grenoble, 2003.
[9] Diffrac Plus: Topas Bruker AXS GmbH, Ostliche, Rheinbruckenstraße, 50, 2006, p. D-76187, (Karlsruhe, Germany).
[10] Powder Diffraction File PDF4 + ICDD (Release 2011).
[11] I. Abrahams, F. Krok, J. Mater. Chem. 12 (2002) 3351.
[12] M. Alga, A. Ammar, R. Essalim, B. Tanouti, F. Mauvy, R. Decourt, Solid State Sci. 7 (2005) 1173.
[13] S. Beg, N.A.S. Al-Areqi, A. Al-Alas, J. Alloys Compd. 479 (2009) 107.
[14] S. Beg, S. Hafeez, N.A.S. Al-Areqi, Phase Transit. 83 (2010) 169.
[15] H.C. Gupta, Archana, V. Luthra, et al., Vib. Spectrosc. 56 (2011) 235.
[16] H.M. Zaki, S.F. Mansour, J. Phys. Chem. Solids 67 (2006) 1643.
[17] R.G. Zakharov, S.A.Petrova, A.E. Udilov, A.N. Petrov, A.I. Vylkov, Patent RU 72329, 2008.
[18] V.M. Zainullina, V.M. Zhukovskii, E.S. Buyanova, Yu.V. Emel'yanova, Russ. J. Inorg. Chem. 52 (2007) 225.